Arabian Journal of Chemistry (2019) 12, 4388–4397

King Saud University

Arabian Journal of Chemistry

www.ksu.edu.sa
www.sciencedirect.com

ORIGINAL ARTICLE

Hydrothermal synthesis of TiO_2/carbon composites and their application for removal of organic pollutants

Marina Maletić [a,*], Marija Vukčević [a], Ana Kalijadis [b], Ivona Janković-Častvan [a], Aleksandra Dapčević [a], Zoran Laušević [b], Mila Laušević [a]

[a] *Faculty of Technology and Metallurgy, University of Belgrade, Karnegijeva 4, 11000 Belgrade, Serbia*
[b] *Vinča Institute of Nuclear Science, University of Belgrade, Mike Petrovića Alasa 12-14, P.O. Box 522, 11000 Belgrade, Serbia*

Received 8 February 2016; accepted 24 June 2016
Available online 1 July 2016

KEYWORDS

Hydrothermal synthesis;
TiO_2/carbon composites;
Photocatalysis;
Pharmaceuticals

Abstract TiO_2/carbon composites were synthesized by hydrothermal carbonization, using titanium isopropoxide and glucose precursor solution to obtain composites with Ti/C molar ratios ranging from 0.05 to 0.30. Characterization of obtained composites was performed by thermogravimetric analysis, scanning electron microscopy, nitrogen adsorption–desorption isotherms, X-ray diffraction, UV–Vis diffuse reflectance spectroscopy and Fourier transform infrared spectroscopy. The possibility of using TiO_2/carbon composites as photocatalysts for UV assisted degradation of methylene blue in aqueous solution and selected pharmaceuticals from multicomponent solution was examined. It was found that increase in the glucose concentration, i.e. increased carbon content, leads to the higher porosity and increase in the share of photocatalytically active anatase phase in obtained TiO_2/carbon composites. Sample obtained from the most concentrated glucose solution (TiO_2/HTC_4), showed the superior photocatalytic activity under UV irradiation toward both methylene blue and selected pharmaceuticals. In addition, TiO_2/HTC_4 show high recycling ability with degradation ratio of methylene blue higher than 81% after five cycles. Also, TiO_2/HTC_4 is expected to be a promising candidate for photocatalytic processes using visible light.

1. Introduction

Organic pollutants (drugs, pesticides and organic dyes) have gained increasing attention due to their frequent detection in wastewaters, surface and ground waters. As emerging contaminants, pharmaceuticals can be found in the aquatic environment, usually in the very low concentration (Grujić et al., 2009; Jauković et al., 2014; Rivera-Utrilla et al., 2013), even though, they can cause detrimental effects, such as morphological and metabolic alterations on aquatic organisms and induction of antibiotic resistance in pathogenic microorganism. Therefore, they

* Corresponding author. Fax: +381 113370387.
E-mail addresses: mvukasinovic@tmf.bg.ac.rs (M. Maletić), marijab@tmf.bg.ac.rs (M. Vukčević).
Peer review under responsibility of King Saud University.

Production and hosting by Elsevier

http://dx.doi.org/10.1016/j.arabjc.2016.06.020
1878-5352

should be removed from the water by appropriate purification method. Standard purification methods such as chemical precipitation and coagulation, or adsorption onto organic and inorganic materials could only remove a part of organic pollutants (Sirés and Brillas, 2012). On the other hand, organic pollutants can be efficiently removed from polluted water by photocatalytic processes (Abdennouri et al., 2013; Ahmed et al., 2011; Kim et al., 2012; Zaccariello et al., 2014), in the presence of different photocatalysts. Titanium dioxide (TiO_2) is one of the most effective and the most commonly used photocatalysts, due to good stability, high activity, little harmfulness to humans, easy availability and low cost (Kim et al., 2012; Zhao et al., 2010a). Unfortunately, due to its relatively high band-gap energy, TiO_2 can be excited only by ultraviolet (UV) light (Kim et al., 2012). Better photocatalytic activity of TiO_2 in the visible region can be achieved by doping the TiO_2 with metals and non-metals, and consequently moving the energy gap to lower energy value (Dolat et al., 2012; Leary and Westwood, 2011; Pelaez et al., 2012; Tan et al., 2012; Wang et al., 2009). Also, highly reactive photocatalysts can be obtained by combining titanium dioxide with different carbon materials, as a catalyst carrier (Belayachi et al., 2019; Czech and Buda, 2015; Maletić et al., 2015; Pastrana-Martínez et al., 2012). For example, Belayachi et al. (2019) used powdered grape marc-based activated carbon impregnated with titanium dioxide for removal of reactive black 5 dye from aqueous solutions, while Pastrana-Martínez et al. (2012) have used graphene oxide–TiO_2 composites for photocatalytic degradation of diphenhydramine pharmaceutical and methyl orange dye. Czech and Buda (2015) obtained photocatalytically active multiwall-carbon nanotubes–TiO_2–SiO_2 nanocomposites for degradation of Bisphenol A and carbamazepine. In our previous work, we applied simple thermal treatment method for loading TiO_2 particles on carbon monolith carrier, and produced highly reactive photocatalysts for degradation of methylene blue (Maletić et al., 2015). According to the literature (Abdennouri et al., 2013; Bestetti et al., 2010; Carpio et al., 2005), one of the most commonly used methods for loading the TiO_2 particles on carbon material is a sol–gel method. Although catalyst obtained in this way has good photocatalytic activity, sol–gel method is time-consuming process, which is its main disadvantage. Relatively new method for the preparation of TiO_2/carbon composites is hydrothermal carbonization. Yang et al. (2015) used hydrothermal synthesis for producing photocatalytically active surface fluorinated TiO_2/reduced graphene oxide nanocomposites for degradation of estrogens, while Zhao et al. (2010b) used one step solvothermal method for preparation of carbon@TiO_2 composites for visible light photocatalytic degradation of methyl orange.

In this work TiO_2/carbon composites were obtained by hydrothermal carbonization using glucose and titanium isopropoxide as a C and Ti precursors, respectively. TiO_2/carbon composites with different Ti/C molar ratios were used as a photocatalyst in the process of removing organic pollutants from aqueous solution. Photocatalytic activities of TiO_2/carbon composites were examined in the process of photocatalytic degradation of methylene blue (MB) and pharmaceuticals selected from different classes: painkillers (diclofenac), antibiotics (azithromycin, doxycycline, erythromycin), sedatives (bromazepam) and cardiovasculars (atorvastatin, amlodipine, cilazapril, simvastatin, clopidogrel). To the best of our knowledge, hydrothermally obtained TiO_2/carbon composites have not been used yet for photocatalytic degradation of pharmaceuticals from multicomponent solution. Based on photocatalytic performance of TiO_2/carbon composites, the most promising carbon composite with high absorptive capabilities for photocatalytic degradation was selected, and its photocatalytic activity under visible irradiation was tested.

2. Experimental

2.1. Sample preparation

Hydrothermal synthesis of TiO_2/carbon composites (TiO_2/HTC) was carried out using the following procedure: 37 ml solution of glucose was mixed with 3 ml 35% hydrochloric acid and 6 ml of titanium isopropoxide was added dropwise. Different concentrations of glucose solution: 5, 10, 15 and 30 g dm^{-3} were used to achieve following Ti/C molar ratio in suspension: 0.05; 0.1; 0.15 and 0.30; the obtained samples were marked as TiO_2/HTC_1, TiO_2/HTC_2, TiO_2/HTC_3 and TiO_2/HTC_4, respectively. The characteristics of the obtained TiO_2/HTC composites were compared with the characteristics of TiO_2 – hydrothermal, obtained by similar procedure, using 37 ml of water instead of glucose solution. The suspension was transferred into 50 ml Teflon lined stainless steel autoclave where hydrothermal carbonization is carried out at temperature at 160 °C and self-generated pressure for 12 h. After completion of the reaction, autoclave cooled to room temperature and suspension was centrifuged. The resulting precipitate was filtrated and washed with distilled water and ethanol several times, and finally dried at 60 °C overnight.

2.2. Sample characterization

The thermogravimetric (TG) analysis was performed on an SDT Q600 instrument (TA Instruments) in O_2 atmosphere (flow rate: 100 cm^3 min^{-1}; heating rate: 20 °C min^{-1}), ranging from room temperature to 800 °C.

The morphology and the surface properties of the obtained materials were investigated by scanning electron microscopy (SEM) using a Mira Tescan 3X at 20 keV.

Nitrogen adsorption–desorption isotherms were determined using a Micromeritics ASAP 2020 instrument. The specific surface area of samples was calculated according to the Brunauer, Emmett, Teller (BET) method from the linear part of the nitrogen adsorption isotherms. The total pore volume (V_{tot}) was given at $p/p_0 = 0.998$. Pore size distribution and volume of the mesopores (V_{meso}) were estimated by applying the Barrett, Joyner and Halenda method from the desorption branch of isotherm. The volume of micropores (V_{micro}) was calculated from alpha-S plot.

In order to study the crystal modifications of the TiO_2 X-ray diffraction (XRD) was used. XRD spectra were recorded in the range of 2θ of 20–60° with a scan speed 1 °C min^{-1} using a Philips PW1710 diffractometer with CuKα radiation.

UV–Vis diffuse reflectance spectroscopy (DRS) was used to examine the effect of precursor molar ratio on the shift of energy band gap of TiO_2 to the visible region. The spectra of the obtained materials were recorded on a Shimadzu 2600 UV–VIS spectrophotometer with an integrating sphere in the range of 220–750 nm, using $BaSO_4$ as a reference.

Fourier transform infrared spectroscopy (FT-IR) measurements were used for characterization of functional groups. FT-IR spectra were recorded in the range from 400 to 4000 cm^{-1} on Bomem MB-Series, Hartmann Braun.

2.3. Measurement of photocatalytic activity

The photocatalytic activity of the TiO_2/HTC composites was examined in the degradation process of methylene blue (MB). All experiments were performed at room temperature with 1 g dm^{-3} of TiO_2/HTC composites and the initial concentration of MB was 10 mg dm^{-3}. The suspension was magnetically stirred in the dark for 60 min to establish the adsorption/desorption equilibrium, and then exposed to the

UV light irradiation using 125 W high-pressure mercury lamp (Philips, HPLN, emission bands in the UV region at 304, 314, 335 and 366 nm, with maximum emission at 366 nm). UV lamp was located at 10 cm above the solution. The entire process of adsorption and decomposition lasted 5 h under constant stirring. The possibility of reusing TiO_2/HTC composites was examined through the determination of photocatalytic activity of sample TiO_2/HTC_4 after each of five cycles. After finishing a cycle, sample TiO_2/HTC_4 was rinsed and dried in the atmosphere, without any other treatments, and then used in next cycle. Photocatalytic activity of sample TiO_2/HTC_4 in the visible light was tested through photocatalytical degradation of MB, under the same experimental conditions. For this purpose 150 W tungsten halogen lamp was used and short wavelength components (λ < 420 nm) of the light were cut off using a glass optical filter. During the process of photocatalytic degradation, at given time intervals, samples were taken and filtered through the 0.45 μm PVDF filters, and then concentration of MB was measured. In the case of sample TiO_2/HTC_4, additional desorption experiment was performed, after the adsorption and photocatalytic experiments were completed. MB, remained on the sample surface after the adsorption and photocatalytic experiments, was desorbed by methanol in the batch system with constant shaking. Concentration of MB was measured using visible spectrophotometer (Specol, Carl-Zeiss, Jena), by measuring absorbance at 675 nm.

Also, photocatalytic activity of the TiO_2/HTC composites was examined in the degradation process of selected pharmaceuticals from multicomponent solution. Initial concentration for each of selected pharmaceuticals: diclofenac, azithromycin, doxycycline, erythromycin, bromazepam, atorvastatin, amlodipine, cilazapril, simvastatin and clopidogrel were 100 μg dm^{-3}. All experiments, photocatalytic degradation under UV irradiation and desorption experiments on TiO_2/HTC_4, were performed under the similar conditions, as described for MB experiments. Concentration of pharmaceuticals was measured by high performance liquid chromatography-tandem mass spectrometry (LC-MS/MS Thermo Scientific).

Surveyor HPLC system was used for the separation of the analytes on the reverse-phase Zorbax Eclipse XDB-C18 column, 75 mm long, 4.6 mm i.d. and 3.5 μm particle size (Agilent Technologies). The mobile phase consisted of water (A), methanol (B) and 10% acetic acid (C) and gradient changes are shown in Fig. 1. An aliquot of 10 μl of the aqueous solution was injected into HPLC system. Linear ion trap mass spectrometer, LTQ XL, was used for detection and quantification of pharmaceuticals. The electrospray ionization technique was used and all pharmaceuticals were analyzed in the positive ionization mode. From obtained MS^2 spectra of pharmaceuticals, most abundant fragment ions were selected. The selected reaction monitoring (SRM) mode was used for quantification of all pharmaceuticals. Mass chromatogram of selected pharmaceuticals is shown in Fig. 2.

3. Results and discussion

3.1. Characterization of photocatalysts

Thermogravimetric analysis (TG) is used to estimate the TiO_2 and carbon content of hydrothermally synthesized samples, and TG curves of TiO_2 – hydrothermal and TiO_2/HTC composites are shown in Fig. 3. The mass loss for TiO_2 – hydrothermal was 3.37 wt% due to the removal of physically and chemically adsorbed water. For TiO_2/HTC composites, the mass loss up to the temperature of 125 °C is a consequence of physically adsorbed water, while the substantial mass loss observed from 450 °C to 500 °C, depending on the sample, is the result of carbon release during the thermal treatment. Based on the thermal analysis results, TiO_2 and carbon content of TiO_2/HTC composites was calculated and is shown in Fig. 3.

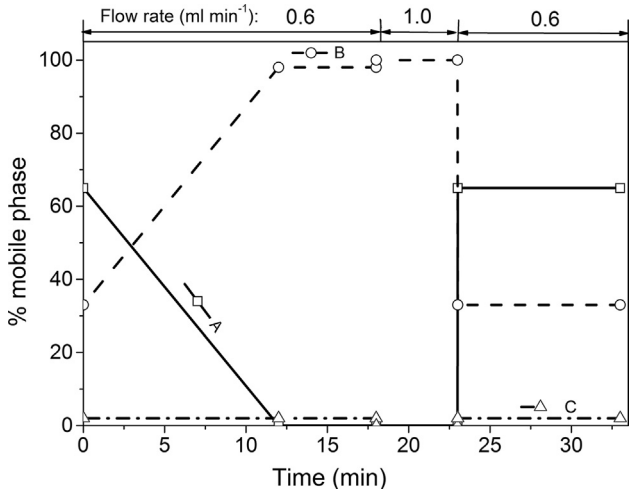

Figure 1 Diagram of the mobile phase composition (A – water, B – methanol and C – 10% acetic acid) and flow rate.

Morphology of obtained TiO_2/HTC composites is shown in Fig. 4. For the purpose of comparison, SEM photographs of TiO_2 – hydrothermal, along with hydrothermal carbon (HTC) derived from glucose are shown in Fig. 4a and f, respectively. The similarity between morphologies of TiO_2/HTC composites and TiO_2 – hydrothermal can be noted, with respect to decrease in particle sizes with the increase in carbon content. On the other hand, HTC poses quite different morphology (Fig. 4f); it is characterized by the presence of large and clearly defined carbon spheres with smooth surface that form cluster-like structure (Sun and Li, 2004; Titirici et al., 2008). Addition of titanium isopropoxide to the glucose solution in order to obtain TiO_2/HTC composites (Fig. 4a–e), induces the morphological changes, in the first place, the disappearance of HTC spherical structure.

Textural properties TiO_2 – hydrothermal and TiO_2/HTC composites are summarized in Table 1. Obtained TiO_2/HTC composites are mesoporous, with the average pore diameter from 3.78 nm, for TiO_2/HTC_4, to 17.22 nm, for TiO_2 – hydrothermal. The results summarized in Table 1 show that average pore diameter and V_{meso} decrease with the increase in carbon content. On the other hand, increase in carbon content leads to the increased S_{BET} and V_{micro}.

XRD analysis was performed in order to analyze crystal phases of TiO_2, present in TiO_2/HTC composites, and to determine phase content and grain size. Also, the influence of precursor ratios (Ti/C), used for hydrothermal synthesis of TiO_2/HTC composites, on the phase formation was examined. The anatase is active form of photocatalyst in the processes of oxidation, while the rutile form is suitable to operate in the

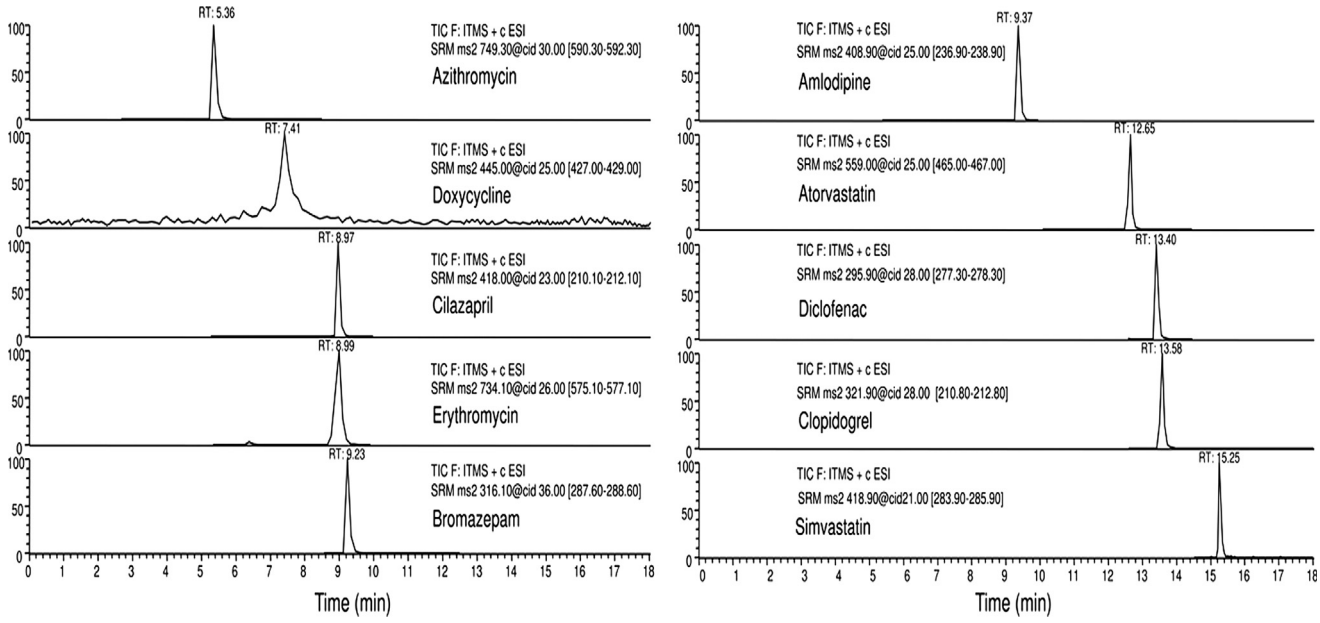

Figure 2 Mass chromatogram of selected pharmaceuticals.

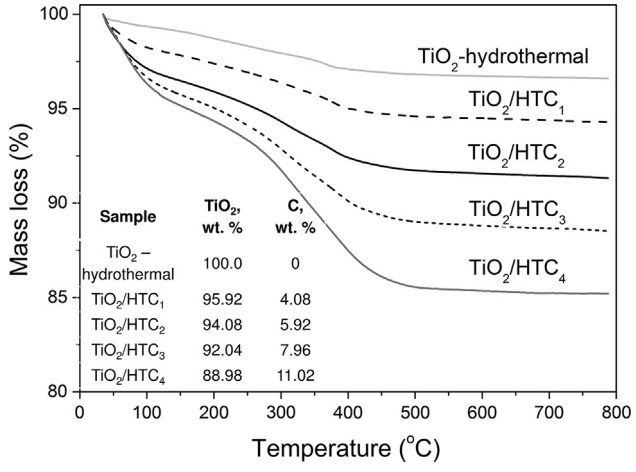

Figure 3 TG curves of TiO_2 – hydrothermal and TiO_2/HTC composites with embedded TiO_2 and carbon content.

near UV range (350–400 nm), because it has a lower energy gap (3.0 eV) than the anatase modification (3.2 eV) (Hanaor and Sorrell, 2011). The presence of TiO_2 in the obtained samples was confirmed by the XRD characteristic peaks for the anatase (101) ($2\theta = 25.6°$) and rutile (110) ($2\theta = 27.7°$) phases (Kordouli et al., 2015). The XRD pattern of TiO_2 – hydrothermal (Fig. 5), shows intense peak at 27.7°, which corresponds to the rutile crystalline phase, and the peak corresponding to the anatase phase (25.6°) of low intensity. XRD diffraction patterns of TiO_2/HTC_1, TiO_2/HTC_2, TiO_2/HTC_3 and TiO_2/HTC_4 (Fig. 5) show that with an increase in the molar ratio of glucose, i.e. increase of carbon content in the material, peak intensity of the anatase phase increases while peak intensity of the rutile phase decreases. This is in accordance with finding of Zhong et al. (2010), that the higher concentration of glucose may be responsible for the formation of anatase phase.

TiO_2 anatase over rutile ratio was calculated from (Zhao et al., 2010a):

$$\text{anatase content}: A\ (\text{wt.}\%) = \frac{100}{1 + 1.265 \cdot (I_R/I_A)}$$

$$\text{rutile content}: R\ (\text{wt.}\%) = 100 - A\ (\text{wt.}\%)$$

with I_A and I_R the diffraction intensities of the anatase (101) and rutile (110) crystalline phases at $2\theta = 25.6°$ and 27.7°, respectively. The average grain size D (nm) was determined from the XRD pattern according to the Debye–Scherrer equation:

$$D = \frac{k\lambda}{\beta \cos\theta}$$

where k is a constant (0.9), λ is the X-ray wavelength (0.15418 nm), β (rad) is the full width at half maximum of the diffraction line, and θ (rad) is the diffraction angle (Tian et al., 2006). The values of β and θ of anatase and rutile were taken from anatase (101) and rutile (211) diffraction line, respectively. Anatase and rutile phase content, and grain sizes of examined samples are summarized in Table 2.

The observed increase in anatase phase with carbon content is confirmed by the results presented in Table 2: anatase content increases from 7.6%, for TiO_2 – hydrothermal, to 76.0%, for TiO_2/HTC_4. It can be noted that ratio of anatase and rutile phase obtained for sample TiO_2/HTC_4 is nearly identical with the ratio of anatase and rutile in photocatalytically active Degussa P25. Therefore, it can be assumed that this sample will be the most efficient in photocatalysis. The average grain size (Table 2) decreases with increase in carbon content: from 22.14 nm (TiO_2 – hydrothermal) to 9.76 nm (TiO_2/HTC_4) which is in a good agreement with the results obtained by scanning electron microscopy. This grain size decrease can be the consequence of inhibitory effect of amorphous carbon on grain growth of TiO_2. In addition, transformation of rutile to anatase phase, with carbon content increase, leads to decrease in grain size. Grain size decrease,

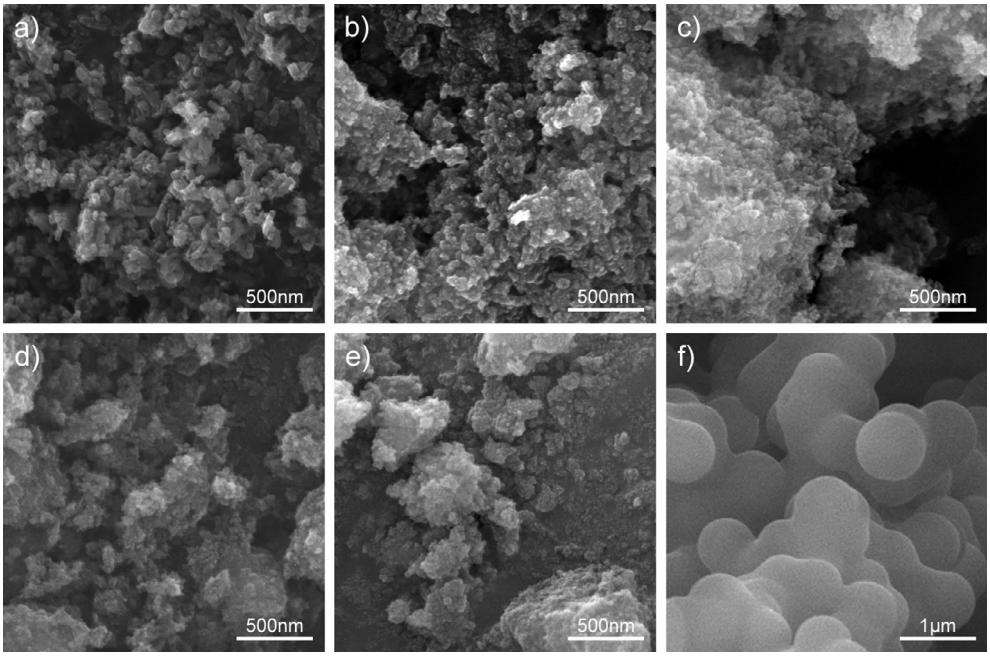

Figure 4 SEM photographs of samples: (a) TiO_2 – hydrothermal; (b) TiO_2/HTC_1; (c) TiO_2/HTC_2; (d) TiO_2/HTC_3; (e) TiO_2/HTC_4 and (f) hydrothermal carbon.

Table 1 Textural properties of examined samples.

Sample	S_{BET} ($m^2\ g^{-1}$)	V_{total} ($cm^3\ g^{-1}$)	V_{meso} ($cm^3\ g^{-1}$)	V_{micro} ($cm^3\ g^{-1}$)	D_{av}[a] (nm)
TiO_2-hydrothermal	49.63	0.2394	0.2375	0.0133	17.22
TiO_2/HTC_1	98.17	0.3290	0.3265	0.0256	10.98
TiO_2/HTC_2	129.01	0.2868	0.2839	0.0349	7.20
TiO_2/HTC_3	154.77	0.2605	0.2573	0.0414	5.25
TiO_2/HTC_4	174.08	0.2048	0.1995	0.0482	3.78

[a] D_{av} – average pore diameter.

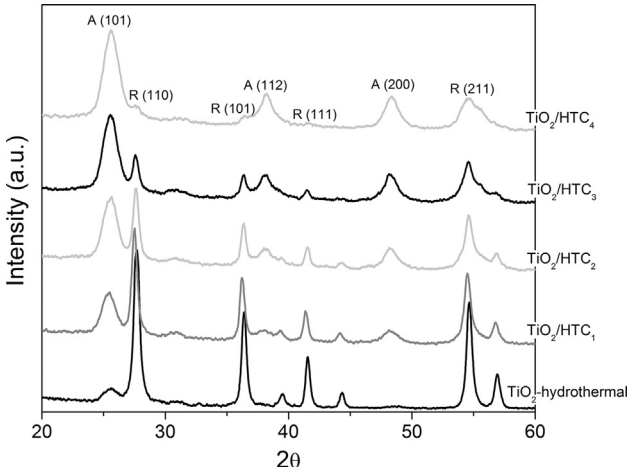

Figure 5 XRD patterns of obtained samples.

accompanied with increase in BET surface area (Table 1), is in very good agreement with the values of average pore diameters (Table 1), indicating that pores measured are most likely interparticle spaces.

Table 2 Anatase and rutile phase content, and grain sizes of examined samples.

Sample	Grain size (nm)			Phase content (wt.%)	
	Anatase	Rutile	Average	Anatase	Rutile
TiO_2-hydrothermal	14.86	29.43	22.14	7.6	92.4
TiO_2/HTC_1	12.72	29.43	21.07	26.0	74.0
TiO_2/HTC_2	11.42	17.66	14.54	41.8	58.2
TiO_2/HTC_3	11.18	12.71	11.94	57.8	42.2
TiO_2/HTC_4	11.18	8.35	9.76	76.0	24.0

UV–Vis DRS spectra show the optical properties of different TiO_2/HTC composites. For the purpose of comparison, the UV–Vis DRS spectra of commercial TiO_2 (anatase) and TiO_2 – hydrothermal were also recorded. TiO_2 – hydrothermal (Fig. 6), containing rutile phase, shows the absorption of radiation in the wavelength range up to 440 nm, while the commercial titanium dioxide, which contains anatase phase, absorbs radiation of wavelengths up to 410 nm. On the other hand, TiO_2/HTC composites absorb

radiation into the wider area of wavelengths, up to 750 nm. For TiO_2/HTC composites (Fig. 6), sample TiO_2/HTC_4 shows the highest absorption of radiation in the visible light region, while TiO_2/HTC_1 shows the lowest absorption. Observed increase in absorption of radiation with the carbon content in the material (Fig. 6) may be the consequence of the absorption of radiation in the visible light region by the carbon present in the obtained samples (Dong et al., 2009; Ren et al., 2007). Also, the reduction in glucose employed in the hydrothermal process may lead to carbonaceous species embedded in the TiO_2 matrix. This substitutional carbon could narrow the band gap of TiO_2 and make the catalyst to absorb visible light efficiently (Lin et al., 2011; Zheng et al., 2015). Considering that the samples of TiO_2/HTC composites absorb radiation in the wavelength area of 220–750 nm, it can be expected that obtained TiO_2/HTC composites, especially TiO_2/HTC_4, may be photocatalytically active in the visible region.

FT-IR spectra of examined TiO_2/HTC composites, along with the FT-IR spectra of HTC, TiO_2 – commercial and TiO_2 – hydrothermal, are shown in Fig. 7. For hydrothermal carbon (Fig. 7a), the wide band between 3000 and 3400 cm^{-1}, is assigned to the stretching vibrations of O—H in hydroxyl or carboxyl groups. The bands around 2815–3000 cm^{-1} are the characteristic stretching vibrations of aliphatic C—H, while the absorption band near 1710 cm^{-1} is attributed to stretching vibration of —C═O from carbonyl and carboxyl groups. The out-of-plane bending vibration of aromatic C—H bands was observed in the region of 750–875 cm^{-1} (Fig. 7a), and the band at 1620 cm^{-1} is attributed to the C═C vibrations (Chen et al., 2012; Sevilla and Fuertes, 2009), suggesting the aromatization of the material during the hydrothermal treatment. For titanium dioxide (hydrothermal and commercial) (Fig. 7b), the strong intensity of the absorption peak at about 3400 cm^{-1} may correspond to the stretching vibration of adsorbed water and hydroxyls on the surface of TiO_2 and the peak at about 1630 cm^{-1} derives from the bending vibration of the O—H bond in hydroxyls and adsorbed water (Shen et al., 2015; Wang et al., 2012; Yu and Shi, 2010). For all TiO_2/HTC composites (Fig. 7c) FT-IR spectra are similar and show a wide hydroxyl stretching vibration mode in carboxyl, phenol and/or intercalated H_2O (ν O—H) at 3400 cm^{-1}, and skeletal vibrations assigned to the components from the oxygen parched carbon domains (δ C═C) at 1620 cm^{-1} (Kalijadis et al., 2015). According to the literature (Dong et al., 2009; Huang et al., 2008), the surface hydroxyl groups can be trapped by the holes generated under UV light irradiation to form hydroxyl radicals which can suppress electron-hole recombination and increase photocatalytic efficiency. Therefore, adsorbed water and hydroxyls represent an important parameter for enhancing the photocatalytic activity (Wang et al., 2012). The highest intensity peaks at 1630 and 3400 cm^{-1}, observed for sample TiO_2/HTC_4 (Fig. 7c), make it the most promising photocatalyst in the process of photocatalytic degradation.

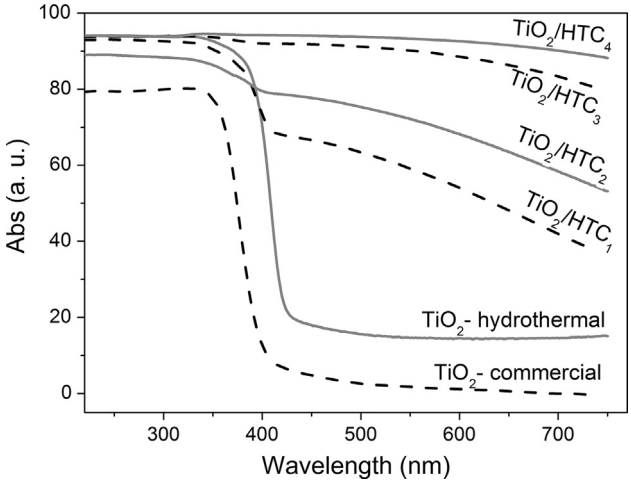

Figure 6 DRS spectra of samples: TiO_2 – hydrothermal, TiO_2 – commercial and TiO_2/HTC composites.

3.2. Photocatalytic activity

The process of removing MB in the presence of TiO_2/HTC composites (shown in Fig. 8) takes place in two phases. The first phase involves the removal of MB by adsorption in the dark, while the second phase represents photocatalytic degradation of MB under UV irradiation. TiO_2 – commercial showed the highest efficiency in photocatalytic degradation of MB, due to the presence of photocatalytically active anatase phase, while TiO_2 – hydrothermal, which mainly contains photocatalytically inactive rutile phase (Fig. 5), showed the lowest efficiency in degradation of MB. As it can be observed (Fig. 8), for all TiO_2/HTC composites, sample TiO_2/HTC_4 showed the highest adsorption capacity and photocatalytic activity toward MB. In addition, for the shorter time of photocatalytic degradation, sample TiO_2/HTC_4 shows much higher photocatalytic activity than TiO_2 – commercial, and that is of great importance in the case of using these materials for the process of water purification. The increase in adsorption and photocatalytic activity (Fig. 8) with the increase in carbon content is observed for all TiO_2/HTC composites. Carbon species present in TiO_2/HTC composites can provide more active sites and adsorb more reactive species due to large surface area and pore volume, which causes the enhanced photocatalytic activity (Lin et al., 2011). It was reported (Kim et al., 2012; Maletić et al., 2015) that high level of MB adsorption on the carbon carrier surface, elevates the photocatalytic activity of TiO_2/HTC composites due to photocatalytic degradation of more accessible, adsorbed MB. After the degradation, carbon surface is again available for adsorption, which elevates the photocatalytic activity of TiO_2/HTC composites and therefore improves its efficiency in MB removal. As it was already mentioned, increased carbon content in TiO_2/HTC composites leads to higher specific surface area (Table 1) and the higher level of adsorption (Fig. 8), and a direct dependence between porous properties and amount of MB adsorbed in the dark can be demonstrated. Therefore, sample TiO_2/HTC_4 showed superior photocatalytic activity in the overall process of MB removal, due to the highest specific surface area and MB adsorption, as well as the presence of photocatalytically active anatase phase. Additionally, high photocatalytic activity of TiO_2/HTC_4 can be explained by the ratio of anatase and rutile phase (Table 2) which is nearly identical with the ratio of anatase and rutile in photocatalytically active Degussa P25.

Photocatalytic degradation of MB on TiO_2/HTC_4 was presented in UV–Vis absorption spectra of MB aqueous

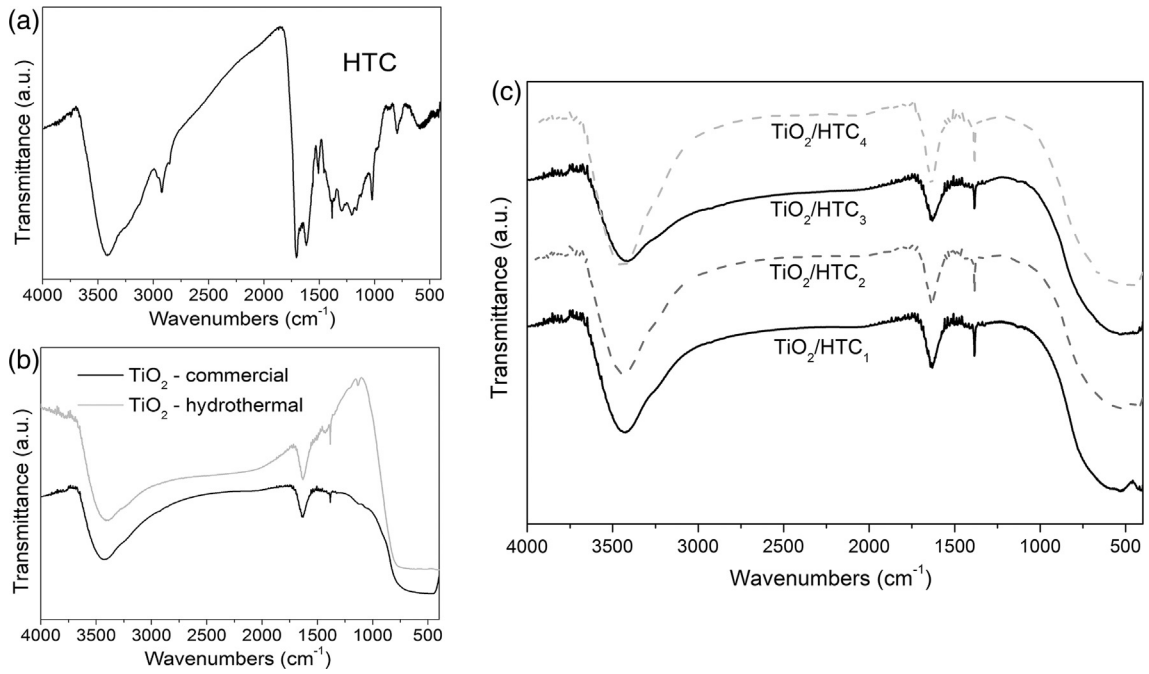

Figure 7 FT-IR spectra of samples: (a) HTC, (b) TiO_2 – commercial, TiO_2 – hydrothermal and (c) TiO_2/HTC composites.

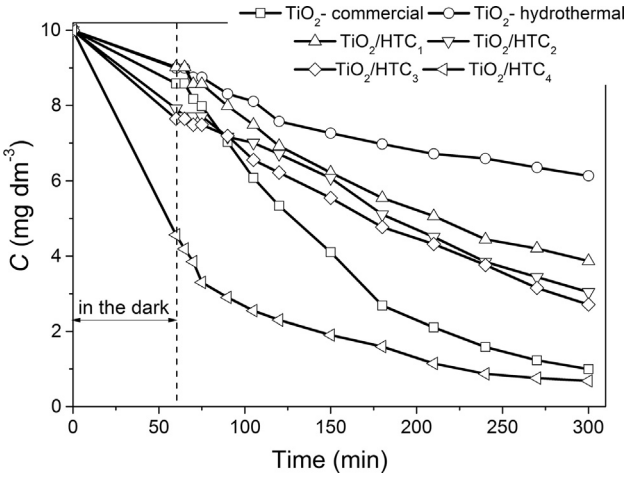

Figure 8 Photocatalytic degradation of MB monitored as the concentration decrease versus time in the presence of TiO_2 and TiO_2/HTC composites under UV light.

solution under different reaction times (Fig. 9). As shown in Fig. 9, the absorption spectrum of the original solution (t = 0 min) shows four peaks around 290, 323, 660 and 605 nm. During the photocatalytic degradation of MB, absorption peak around 660 nm decreased rapidly with a blue-shift of the maximum absorbance peak from 660 to 620 nm. In addition, the absorbance peaks around 605, 323 and 290 nm declined obviously, which indicate that the whole conjugated chromophore structure of MB is destroyed (Yang et al., 2012; Xiong et al., 2012). This confirms the photodegradation of MB in the presence of TiO_2/HTC_4 composite.

The kinetics study of photocatalytic degradation of MB was examined by Langmuir–Hinshelwood kinetic model (Hamad et al., 2016) given by equation:

$$\ln\frac{C_0}{C_t} = k_{app} \cdot t$$

where C_0 is the initial concentration of MB, C_t is the concentration of MB at time t and k_{app} is rate constant. A plot of $\ln\frac{C_0}{C_t}$ versus time in Fig. 10 represents a straight line, with the slope of linear regression equals to the apparent first order rate constant k_{app}. The values of k_{app} obtained for all tested samples are given in Table 3. With increasing carbon content, the photocatalytic activity of TiO_2/HTC composites increases, and TiO_2/HTC_4 showed the highest activity with the apparent reaction rate constant (k_{app}, 0.0102 min^{-1}) higher than that of TiO_2 – commercial (k_{app}, 0.0070 min^{-1}). According to the literature (Dong et al., 2009;Jin et al., 2016; Wang et al., 2015), apparent reaction rate

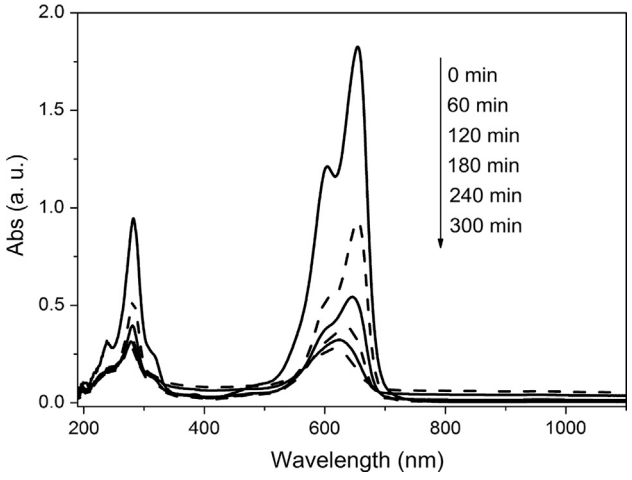

Figure 9 UV–Vis absorption spectra of MB aqueous solution under different reaction times.

constant, obtained for TiO_2/HTC_4, is comparable, or even higher than that obtained for different carbon modified TiO_2 photocatalysts and Degussa P25.

Since adsorption and photocatalytic degradation occur simultaneously, the amount of MB degraded on TiO_2/HTC_4 can be determined by subtracting the amounts of not degraded MB, remained in solution and on the TiO_2/HTC_4 surface after photocatalytic experiment, from the initial amount of MB. For that purpose, MB desorption test was performed after photocatalytic experiment. After adsorption in the dark, sample TiO_2/HTC_4 adsorbed 54.4% of the initial MB amount in the solution (0.5 mg MB) (Fig. 8). After the photocatalytic experiment, 0.021 mg MB was desorbed from the sample surface, while 0.034 mg MB remained in the solution. These results indicate that nearly all of the adsorbed MB was subsequently photocatalytically degraded on the TiO_2/HTC_4 surface, simultaneously releasing the surface active cites for a new adsorption followed by photocatalytic degradation.

The regeneration and recycling of TiO_2 photocatalysts is one of key steps in practical applications of this heterogeneous photocatalysis in water purification. Therefore, an examination of the photocatalytic activity of the recycled TiO_2/HTC_4 was carried out under UV light irradiation. The results are shown in Fig. 11. The degradation rate in first cycle was 91.9%, while after five cycles degradation rate was decreased to 81.2%.

The possibility of using TiO_2/HTC_4 as a photocatalyst in the visible light was tested through the photocatalytic degradation of MB. Obtained results (Fig. 12) showed that UV irradiation induces a higher decrease in MB concentration than the visible light. Nevertheless, concentration of MB was decreased for about 70% in the presence of TiO_2/HTC_4 and visible irradiation. Therefore, it can be said that TiO_2/HTC_4 showed satisfactory photocatalytic activity under the visible light.

Obtained results suggest that TiO_2/HTC composites with higher carbon content can be successfully applied in degradation of organic pollutants. Therefore, TiO_2/HTC composites were utilized as a photocatalysts for photocatalytic degradation of pharmaceuticals from the multicomponent solution. Percentage of pharmaceuticals adsorbed in the dark and subsequently photocatalytically degraded in the presence

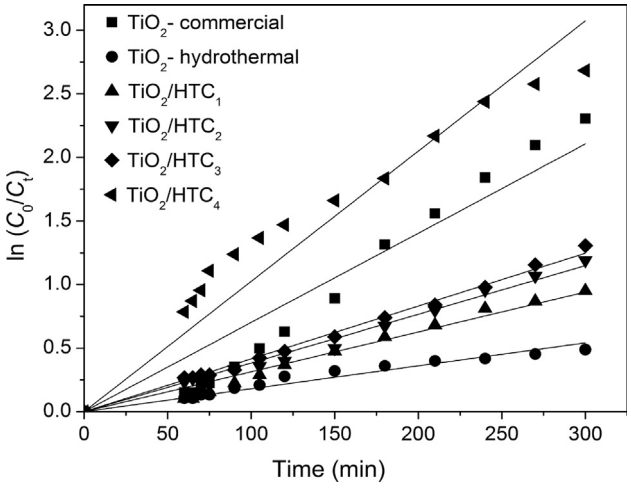

Figure 10 Photocatalytic activity of hydrothermally synthesized samples and TiO_2-commercial.

Table 3 Pseudo-first order apparent constant values for MB degradation.

Sample	$k_{app} \times 10^2$, (min^{-1})	R^2
TiO_2 – hydrothermal	0.18	0.988
TiO_2 – commercial	0.70	0.962
TiO_2/HTC_1	0.31	0.989
TiO_2/HTC_2	0.38	0.997
TiO_2/HTC_3	0.41	0.998
TiO_2/HTC_4	1.02	0.981

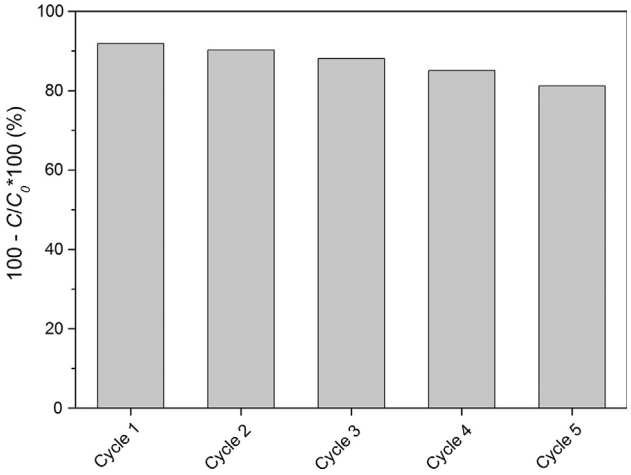

Figure 11 Recycle of the TiO_2/HTC_4 composite for the degradation of MB (initial concentration of MB 10 mg dm^{-3}, 50 ml).

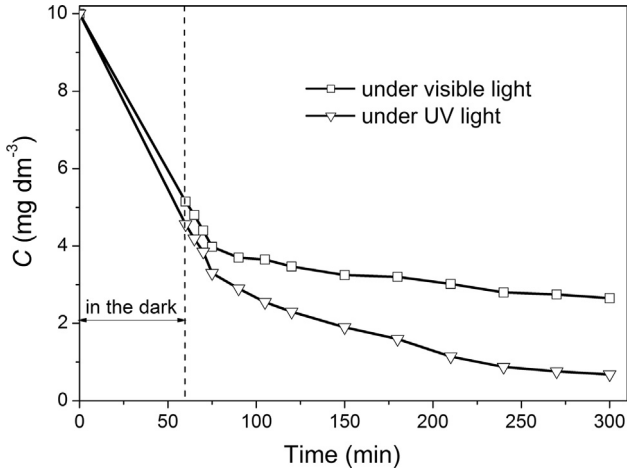

Figure 12 MB removal in the presence of TiO_2/HTC_4 under the UV and visible light.

of TiO_2/HTC composites is presented in Table 4. All tested TiO_2/HTC composites showed both very high levels of adsorption and photocatalytic degradation of azithromycin, atorvastatin, amlodipine, simvastatin and clopidogrel. Generally, the level of adsorption and photocatalytic degradation of azithromycin, doxycycline, bromazepam, atorvastatin and clopidogrel increase with the carbon content. On the other

Table 4 Adsorbed and photocatalytically degraded pharmaceuticals in the presence of TiO_2/HTC composites.

Pharmaceutical	TiO_2/HTC_1		TiO_2/HTC_2		TiO_2/HTC_3		TiO_2/HTC_4	
	Ad[a], %	Re[b], %	Ad[a], %	Re[b], %	Ad[a], %	Re[b], %	Ad[a], %	Re[b], %
Diclofenac	64.8	99.0	84.2	99.3	62.9	96.4	64.4	92.1
Azithromycin	85.3	99.2	94.8	99.1	94.1	98.8	98.9	99.4
Doxycycline	86.7	100	66.6	88.8	79.2	91.3	93.7	100
Erythromycin	65.9	84.9	97.9	99.4	72.2	81.6	72.3	91.7
Bromazepam	39.7	79.3	44.8	81.0	76.0	82.1	84.6	90.8
Atorvastatin	93.9	99.2	97.3	99.8	96.3	98.3	91.2	99.8
Amlodipine	99.3	99.3	97.0	99.8	99.6	99.8	99.8	99.8
Cilazapril	23.3	85.0	21.8	79.1	25.9	70.7	26.8	76.5
Simvastatin	98.5	98.8	98.3	99.5	99.3	100	98.8	98.9
Clopidogrel	70.3	97.4	96.7	97.7	93.4	99.2	92.8	98.7

[a] Ad – Adsorbed.
[b] Re – Removed.

hand, it seems that carbon content does not affect the adsorption and photocatalytic degradation of diclofenac, erythromycin and cilazapril. Also, for all tested composites, level of cilazapril adsorption was the lowest, but after UV irradiation about 75% of cilazapril was photocatalytically degraded. This behavior may be the consequence of low affinity toward composite surface and slow adsorption, followed by good photocatalytic degradation of cilazapril. Obtained results indicate superior photocatalytic activity of TiO_2/HTC_4 in pharmaceutical removal from multicomponent solution. The amounts of pharmaceuticals degraded on the surface of TiO_2/HTC_4 were determined in the similar manner as in MB desorption test. The lowest level of subsequent photocatalytic degradation was observed for erythromycin and bromazepam: about 87% of erythromycin and 40% of bromazepam adsorbed on the surface of TiO_2/HTC_4 were subsequently photocatalytically degraded. In the case of diclofenac, cilazapril, simvastatin and clopidogrel, more than 93% of adsorbed pharmaceuticals are photocatalytically degraded. Nevertheless, complete subsequent photocatalytic degradation of pharmaceuticals adsorbed on the surface of TiO_2/HTC_4 was observed for azithromycin, doxycycline, amlodipine and atorvastatin.

4. Conclusions

Photocatalytically active TiO_2/carbon composites were obtained by hydrothermal carbonization, using titanium isopropoxide and glucose as a titanium and carbon precursors, respectively. It was found that photocatalytic activity increases with the concentration of glucose precursor solution, due to the increase in the share of photocatalytically active anatase phase in obtained TiO_2/carbon composites. Also, increase in the carbon content leads to the higher surface area, which synergistically improved the photocatalytic activity of obtained TiO_2/-carbon composites by enhancing the adsorption of the organic pollutants. Consequently, sample TiO_2/HTC_4, obtained from the most concentrated glucose solution, showed the superior photocatalytic activity under UV irradiation toward both methylene blue and selected pharmaceuticals in multicomponent solution. In addition, TiO_2/HTC_4 could be used for multiple degradation cycles with slight decrease in photocatalytic activity, as well as a promising candidate for photocatalytic processes using visible light.

Acknowledgments

The authors wish to thank the Ministry of Education, Science and Technological Development Republic of Serbia for financial support through the project of Basic Research, No. 172007 and Physics and Chemistry with Ion Beams (III) No. 45006.

References

Abdennouri, M., Elmoubarki, R., Elmhammedi, A., Galadi, A., Baâlala, M., Bensitel, M., Boussaoud, A., Elhafiane, Y., Smith, A., Barka, N., 2013. Influence of tungsten on the anatase-rutile phase transition of sol-gel synthesized TiO_2 and on its activity in the photocatalytic degradation of pesticides. J. Mater. Environ. Sci. 4, 953–960.

Ahmed, S., Rasul, M.G., Martens, W.N., Brown, R., Hashib, M.A., 2011. Advances in heterogeneous photocatalytic degradation of phenols and dyes in wastewater: A review. Water Air Soil Poll. 215, 3–29.

Belayachi, H., Bestani, B., Benderdouche, N., Belhakem, M., 2019. The use of TiO_2 immobilized into grape marc-based activated carbon for RB-5 Azo dye photocatalytic degradation. Arab. J. Chem. 12 (8), 3018–3027.

Bestetti, M., Sacco, D., Brunella, M.F., Franz, S., Amadelli, R., Samiolo, L., 2010. Photocatalytic degradation activity of titanium dioxide sol–gel coatings on stainless steel wire meshes. Mater. Chem. Phys. 124, 1225–1231.

Carpio, E., Zuniga, P., Ponce, S., Solis, J., Rodriguez, J., Estrada, W., 2005. Photocatalytic degradation of phenol using TiO_2 nanocrystals supported on activated carbon. J. Mol. Catal. A Chem. 228, 293–298.

Chen, C.M., Zhang, Q., Yang, M.G., Huang, C.H., Yang, Y.G., Wang, M.Z., 2012. Structural evolution during annealing of thermally reduced graphene nanosheets for application in supercapacitors. Carbon 50, 3572–3584.

Czech, B., Buda, W., 2015. Photocatalytic treatment of pharmaceutical wastewater using new multiwall-carbon nanotubes/TiO_2/SiO_2 nanocomposites. Environ. Res. 137, 176–184.

Dolat, D., Quici, N., Kusiak-Nejman, E., Morawski, A.W., Puma, G. L., 2012. One-step, hydrothermal synthesis of nitrogen, co-doped titanium dioxide (N, C-TiO_2) photocatalysts. Effect of alcohol degree and chain length as carbon dopant precursors on photocatalytic activity and catalyst deactivation. Appl. Catal. B Environ. 115–116, 81–89.

Dong, F., Wang, H., Wu, Z., 2009. One-step "green" synthetic approach for mesoporous C-doped titanium dioxide with efficient visible light photocatalytic activity. J. Phys. Chem. C 113, 16717–16723.

Grujić, S., Vasiljević, T., Laušević, M., 2009. Determination of multiple pharmaceutical classes in surface and ground waters by liquid chromatography–ion trap–tandem mass spectrometry. J. Chromatogr. A 1216, 4989–5000.

Hamad, H.A., Sadik, W.A., Abd El-latif, M.M., Kashyout, A.B., Feteha, M.Y., 2016. Photocatalytic parameters and kinetic study for degradation of dichlorophenol-indophenol (DCPIP) dye using highly active mesoporous TiO_2 nanoparticles. J. Environ. Sci. 43, 26–39.

Hanaor, D., Sorrell, C.C., 2011. Review of the anatase to rutile phase transformation. J. Mater. Sci. 46, 855–874.

Huang, Y., Ho, W., Lee, S., Zhang, L., Li, G., Yu, J.C., 2008. Effect of carbon doping on the mesoporous structure of nanocrystalline titanium dioxide and its solar-light-driven photocatalytic degradation of NOx. Langmuir 24, 3510–3516.

Jauković, Z., Grujić, S., Vasiljević, T., Petrović, S., Laušević, M., 2014. Cardiovascular drugs in environmental waters and wastewaters: method optimization and real sample analysis. J. AOAC Int. 97, 1167–1174.

Jin, Z., Duan, W., Duan, W., Liu, B., Chen, X., Yang, F., Guo, J., 2016. Indium doped and carbon modified P25 nanocomposites with highvisible-light sensitivity for the photocatalytic degradation of organic dyes. Appl. Catal. A Gen. 517, 129–140.

Kalijadis, A., ãorđević, J., Trtić-Petrović, T., Vukčević, M., Popović, M., Maksimović, V., Rakočević, Z., Laušević, Z., 2015. Preparation of boron-doped hydrothermal carbon from glucose for carbon paste electrode. Carbon 95, 42–50.

Kim, C.H., Kim, B.H., Yang, K.S., 2012. TiO_2 nanoparticles loaded on graphene/carbon composite nanofibers by electrospinning for increased photocatalysis. Carbon 50, 2472–2481.

Kordouli, E., Bourikas, K., Lycourghiotis, A., Kordulis, C., 2015. The mechanism of azo-dyes adsorption on the titanium dioxide surface and their photocatalytic degradation over samples with various anatase/rutile ratios. Catal. Today 252, 128–135.

Leary, R., Westwood, A., 2011. Carbonaceous nanomaterials for the enhancement of TiO_2 photocatalysis. Carbon 49, 741–772.

Lin, X., Rong, F., Ji, X., Fu, D., 2011. Carbon-doped mesoporous TiO_2 film and its photocatalytic activity. Micropor. Mesopor. Mater. 142, 276–281.

Maletić, M., Vukčević, M., Kalijadis, A., Laušević, Z., Laušević, M., 2015. Photocatalytic performance of carbon monolith/TiO_2 composite. Adv. Mater. Sci. Eng., 8 http://dx.doi.org/10.1155/2015/803492, 2015.

Pastrana-Martínez, L., Morales-Torres, S., Likodimos, V., Figueiredo, J., Faria, J., Falaras, P., Silva, A., 2012. Advanced nanostructured photocatalysts based on reduced graphene oxide–TiO_2 composites for degradation of diphenhydramine pharmaceutical and methyl orange dye. Appl. Catal. B Environ. 123–124, 241–256.

Pelaez, M., Nolan, N., Pillai, S., Seery, M., Falaras, P., Kontos, A., Dunlope, P., Hamiltone, J., Byrnee, J.A., O'Sheaf, K., Entezarig, M., Dionysiou, D., 2012. A review on the visible light active titanium dioxide photocatalysts for environmental applications. Appl. Catal. B Environ. 125, 331–349.

Ren, W., Ai, Z., Jia, F., Zhang, L., Fan, X., Zou, Z., 2007. Low temperature preparation and visible light photocatalytic activity of mesoporous carbon-doped crystalline TiO_2. Appl. Catal. B Environ. 69, 138–144.

Rivera-Utrilla, J., Sánchez-Polo, M., Ferro-García, M.Á., Prados-Joya, G., Ocampo-Pérez, R., 2013. Pharmaceuticals as emerging contaminants and their removal from water. A review. Chemosphere 93, 1268–1287.

Sevilla, M., Fuertes, A.B., 2009. The production of carbon materials by hydrothermal carbonization of cellulose. Carbon 47, 2281–2289.

Shen, P.S., Tseng, C.M., Kuo, T.C., Shih, C.K., Li, M.H., Chen, P., 2015. Microwave-assisted synthesis of titanium dioxide nanocrystalline for efficient dye-sensitized and perovskite solar cells. Sol. Energy 120, 345–356.

Sirés, I., Brillas, E., 2012. Remediation of water pollution caused by pharmaceutical residues based on electrochemical separation and degradation technologies: a review. Environ. Int. 40, 212–229.

Sun, X., Li, Y., 2004. Colloidal carbon spheres and their core/shell structures with noble-metal nanoparticles. Angew. Chem. Int. Ed. 43, 597–601.

Tan, Y.N., Wong, C.L., Mohamed, A.R., 2012. Hydrothermal treatment of fluorinated titanium dioxide: photocatalytic degradation of phenol. Asia-Pac. J. Chem. Eng. 7, 877–885.

Tian, B., Chen, F., Zhang, J., Anpo, M., 2006. Influences of acids and salts on the crystalline phase and morphology of TiO_2 prepared under ultrasound irradiation. J. Colloid. Interf. Sci. 303, 142–148.

Titirici, M.M., Antonietti, M., Baccile, N., 2008. Hydrothermal carbon from biomass: a comparison of the local structure from poly- to monosaccharides and pentoses/hexoses. Green Chem. 10, 1204–1212.

Wang, Y., Huang, Y., Ho, W., Zhang, L., Zou, Z., Lee, S., 2009. Biomolecule-controlled hydrothermal synthesis of C-N-S-tridoped TiO_2 nanocrystalline photocatalysts for NO removal under simulated solar light irradiation. J. Hazard. Mater. 169, 77–87.

Wang, D.H., Jia, L., Wu, X.L., Lu, L.Q., Xu, A.W., 2012. One-step hydrothermal synthesis of N-doped TiO_2/C nanocomposites with high visible light photocatalytic activity. Nanoscale 4, 576–584.

Wang, X., Xue, X., Liu, X., Xing, X., Li, Q., Yang, J., 2015. Synergistic effect of single-electron-trapped oxygen vacancies and carbon species on the visible light photocatalytic activity of carbon modified TiO_2. Mater. Chem. Phys. 153, 117–126.

Xiong, S.F., Yin, Z.L., Yuan, Z.F., Yan, W.B., Yang, W.Y., Liu, J.J., Zhang, F., 2012. Dual-frequency (20/40 kHz) ultrasonic assisted photocatalysis for degradation of methylene blue effluent: synergistic effect and kinetic study. Ultrason. Sonochem. 19, 756–761.

Yang, Y., Zhang, G., Xu, W., 2012. Facile synthesis and photocatalytic properties of Ag–AgCl–TiO_2/rectorite composite. J. Colloid. Interf. Sci. 376, 217–223.

Yang, Y., Luo, L., Xiao, M., Li, H., Pan, X., Jiang, F., 2015. One-step hydrothermal synthesis of surface fluorinated TiO_2/reduced graphene oxide nanocomposites for photocatalytic degradation of estrogens. Mater. Sci. Semicon. Proc. 40, 183–193.

Yu, J., Shi, L., 2010. One-pot hydrothermal synthesis and enhanced photocatalytic activity of trifluoroacetic acid modified TiO_2 hollow microspheres. J. Mol. Catal. A Chem. 326, 8–14.

Zaccariello, G., Moretti, E., Storaro, L., Riello, P., Canton, P., Gombac, V., Montini, T., Rodriguez-Castellon, E., Benedetti, A., 2014. TiO_2–mesoporous silica nanocomposites: cooperative effect in the photocatalytic degradation of dyes and drugs. RSC Adv. 4, 37826–37837.

Zhao, W., Bai, Z., Ren, A., Guo, B., Wu, C., 2010a. Sunlight photocatalytic activity of CdS modified TiO_2 loaded on activated carbon fibers. Appl. Surf. Sci. 256, 3493–3498.

Zhao, B.L., Chen, X., Wang, X., Zhang, Y., Wei, W., Sun, Y., Antonietti, M., Titirici, M.M., 2010b. One-step solvothermal synthesis of a carbon@TiO_2 dyade structure effectively promoting visible-light photocatalysis. Adv. Mater. 22, 3317–3321.

Zheng, P., Li, H.Y., Wu, F., Bai, B., Guan, W.S., 2015. Structure-tunable hydrothermal synthesis of composite TiO_2@glucose carbon microspheres (TiO_2@GCs) with enhanced performance in the photocatalytic removal of acid fuchsin (AF). New J. Chem. 39, 8787–8796.

Zhong, J., Chen, F., Zhang, J., 2010. Carbon-deposited TiO_2: synthesis, characterization, and visible photocatalytic performance. J. Phys. Chem. C 114, 933–939.